Hemodialysis vascular access failure: novel pathophysiological mechanisms and therapeutic strategies

Bezhaeva, T.

Chapter 6

Contribution of bone marrow-derived cells to in situ engineered tissue capsules in a rat model of chronic kidney disease

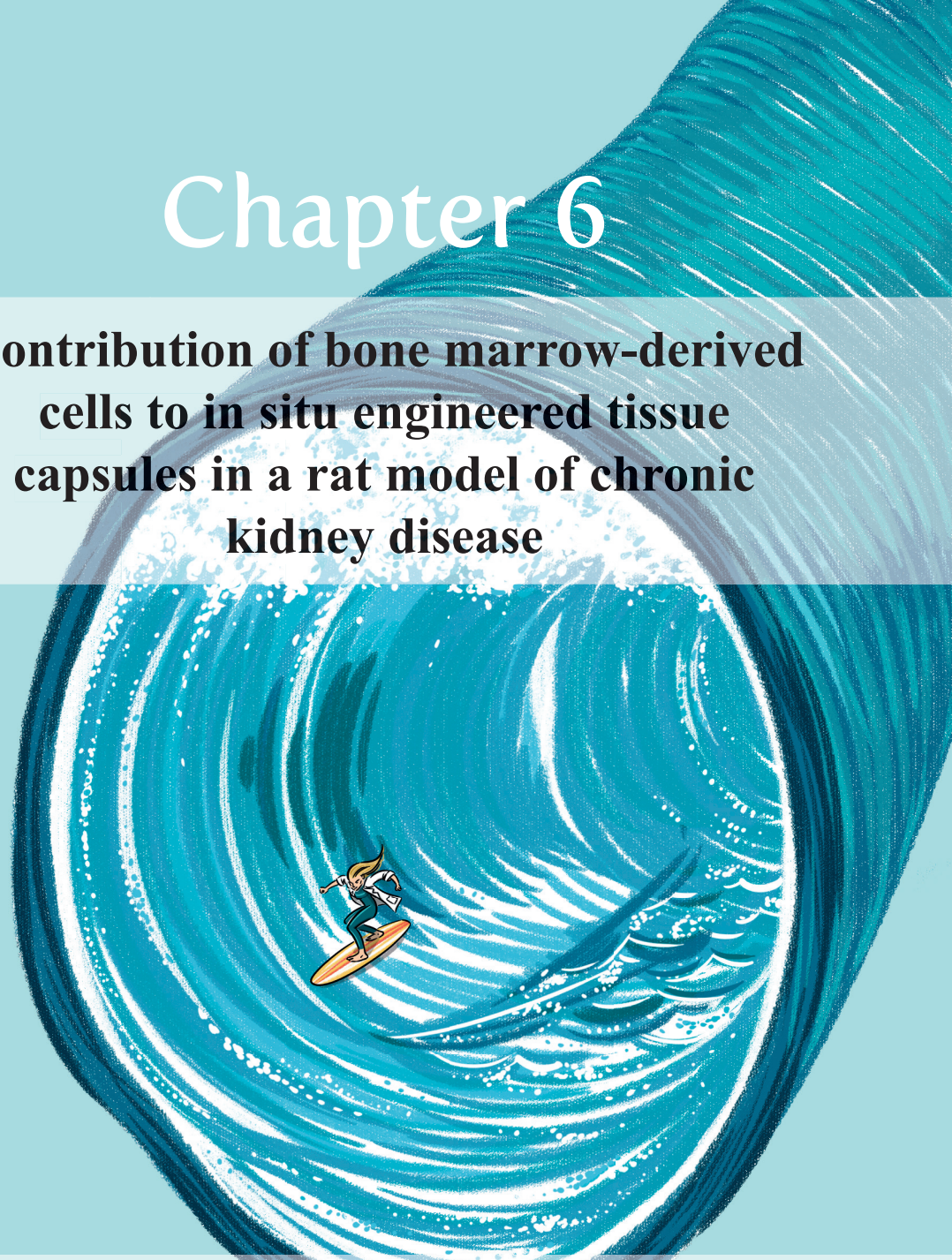

Taisiya Bezhaeva, Wouter J. Geelhoed, Dong Wang, Haoyong Yuan, Eric P. van der Veer, Carla M.A. van Alem, Febriyani F.R. Damanik, Xuefeng Qiu, Anton Jan van Zonneveld, Lorenzo Moroni, Song Li and Joris I. Rotmans

Biomaterials - In press (available online 15 December 2018)

Abstract

Tissue engineered blood vessels (TEBVs) hold great promise for clinical use in patients with end stage renal disease (ESRD) requiring vascular access for hemodialysis. A promising way to make TEBVs is to exploit foreign body response (FBR) of polymeric rods used as templates. However, since the FBR predominantly involves bone-marrow (BM) derived cells and ESRD coincides with impaired function of BM, it is important to assess the generation of TEBVs in conditions of renal failure. To this end, we implanted polymer rods in the subcutis of rats after BM-transplantation with GFP-labeled BM cells in a model of chronic kidney disease (CKD). At 3 weeks after implantation, rods were encapsulated by tissue capsule (TC) composed of collagen, myofibroblasts and macrophages. On average, 13% of $CD68^+$ macrophages were GFP^+, indicating BM origin. Macrophage-to-myofibroblasts differentiation appeared to play an important role in TC formation as 26% of SMA^+/GFP^+ myofibroblasts co-expressed the macrophage marker CD68. Three weeks after rod implantation, the cellular response changed towards tissue repair, characterized by 40% increase in $CD68^+/CD163^+$ repair associated macrophages and 95% increase in TGFβ and IL10 gene expression as compared to TCs harvested at 1 week. These results show that both BM derived and tissue resident cells, contribute to TC formation, whereas macrophages serve as precursors of myofibroblasts in mature TCs. Finally, the presence of CKD did not significantly alter the process of TC formation, which holds the potential to support our approach for future clinical use in ESRD patients.

Clinical problem:

Tissue engineered blood vessels for patients with end stage renal disease requiring vascular access for hemodialysis

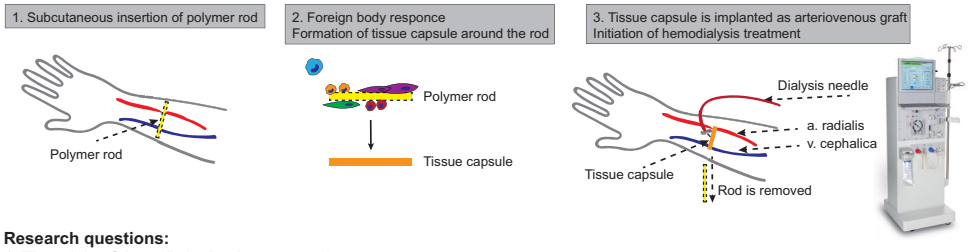

Research questions:

1. The origin of the cells in the tissue capsule
2. Effect of chronic kidney disease on tissue capsule formation

Methods:

Rat model of chronic kidney disease combined with a bone marrow transplantation using GFP-labeled cells

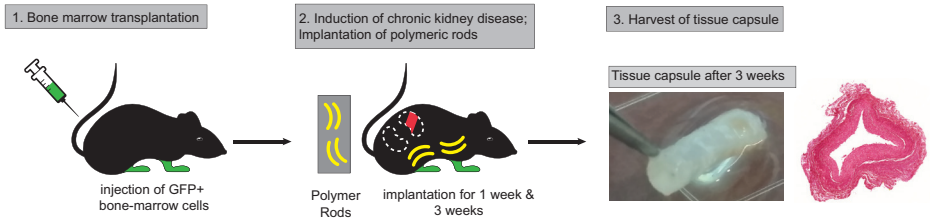

Results:

Cellular origin of cell within the tissue capsule

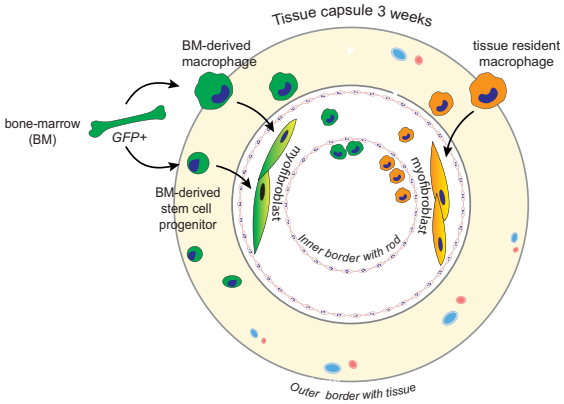

Conclusion:

1. Both bone-marrow derived and tissue resident cells contribute to tissue capsule formation
2. Macrophages serve as precursors of myofibroblasts
3. Chronic kidney disease does not alter process of tissue capsule formation

Introduction

Patients with cardiovascular disease (CVD) or end-stage renal disease (ESRD) frequently require surgery to either replace diseased blood vessels or create a vascular access site for hemodialysis[1-3]. For this purpose, native veins are generally preferred due to superior patency rates when compared to prosthetic grafts, but often unavailable due to preexisting vascular pathology[4,5]. The failure of synthetic vascular grafts predominantly results from the development of intimal hyperplasia ultimately leading to graft occlusion, and a relatively high risk of infectious complications[6-8]. In recent years, various strategies to create tissue engineered vascular grafts have been developed in an effort to overcome current limitations of synthetic grafts and diseased native blood vessels[9-11]. Indeed, tissue engineered blood vessels (TEBVs) can be tailor-made, do not have inconvenient valves and side-branches, are free from pre-existing vascular diseases and have the potential to adapt to changing hemodynamic conditions.

Our approach to generate autologous TEBVs *in vivo* is based on the foreign body response (FBR) directed to a subcutaneously implanted polymer rod that culminates in the formation of a fibrocellular tissue capsule (TC), that encapsulating the rod[12]. Upon extraction of the polymer rod several weeks after implantation, the remaining TC is grafted into the vasculature, whereupon it differentiates into a blood vessel. In this approach, the subcutaneous space is utilized as an *in situ* bioreactor to grow a completely autologous blood vessel. In a previous study in pigs, we demonstrated that upon vascular grafting, the TCs phenotypically differentiate towards a blood vessel, as demonstrated by enhanced matrix synthesis, differentiation of fibroblasts toward contractile vascular smooth muscle cells (VSMCs) and endothelialization of the luminal surface[13].

The dynamics of the FBR to implanted materials have been elucidated in detail[14]. The early phase of the FBR is characterized by the recruitment of inflammatory cells, which is followed by the formation of granulation tissue, ultimately resulting in a fibrocellular TC, which completely encapsulates the implanted foreign body[15]. However, the origin of the cells present within the TCs is still unknown. Understanding the origin of cells present in the TC is of vital importance for its application as vascular grafts, as various disease conditions such as diabetes mellitus, chronic kidney disease (CKD) and ischemic peripheral arterial disease coincide with impaired function of bone marrow (BM)-derived cells[16-18], which could hamper TC formation.

In the present study, we aimed to elucidate the contribution of BM-derived cells in TC formation in a rat model of green fluorescent protein (GFP) BM transplantation[19]. Furthermore, we combined this model with a model of CKD to investigate its effect on TC composition.

Material and Method

Study design

All the animal work was performed at the University of California, Los Angeles and

approved by the institutional animal care and use committee. Five-weeks old male Sprague Dawley (SD) rats (200-250 g) were purchased from Jackson Laboratory (USA) (n=27), transgenic enhanced GFP SD rats (SD-Tg(UBC-EGFP)2BalRrrc) were purchased from rat resource and resource center (University of Missouri, Columbia, USA) (n=9). All animals were housed in the local facilities accredited by the American Association for Accreditation of Laboratory Animal Care and were maintained under controlled conditions of light, temperature, and humidity.

Bone marrow transplantation

After 1-week acclimatization to the new environment, SD-Tg(UBC-EGFP)2BalRrrc rats were used as donor rats for the extraction of bone marrow cells (BMCs). BMCs were harvested from the femurs and tibias of 6 to 8-weeks-old SD-Tg(UBC-EGFP)2BalRrrc rats and the nucleated cells were enriched by lysing red blood cells with Red blood cell lysis buffer (1.2 mL, Sigma, St Louis, MO, USA). The recipient SD rats were lethally irradiated with two apart doses of 5.5 Gy each (11 Gy in total) with a 4h brake using a cobalt-60 gamma source. BMCs ($2*10^7$) were injected via tail vein into recipient rats 24 hours after irradiation. To prevent infections after BM transplantation antibiotic sulfamethoxazole and trimethoprim (0.5 mg/kg) was administrated via the drinking water for 12 days post transplantation. Three weeks after BM reconstitution peripheral blood (0.2 mL) was collected from the tail vein to determine enrichment in GFP^+ cells by fluorescence-activated cell sorting (FACS) analysis.

Model of chronic kidney disease

All operations were performed under isoflurane anesthesia. Three weeks after BM transplantation rats were randomly divided into two experimental groups: healthy controls (n=10) and rats with CKD (n=17). CKD was induced by two-stage subtotal nephrectomy (uninephrectomy of left kidney (UNX) followed 7 days later by 2/3 removal of right kidney), as described previously[20,21]. Two weeks later CKD was confirmed by measuring serum creatinine and blood urea nitrogen (BUN).

Implant material

Solid cylindrical-shaped rods composed of the elastomeric co-polymer PEOT/PBT of 1.75 – 0.25 mm in diameter and 1.5 cm in length were fabricated with a rapid prototyping unit[33] (Envisiontec GmbH, Gladbeck, Germany) used as melt extruder. Rods were composed of the co-polymer poly(ethylene oxide terephthalate)epoly(butylene terephthalate) (PEOT/PBT, Polyvation, The Netherlands), with a PEOT/PBT weight percentage of 55/45 and 300 g/mol molecular weight of the initial polyethylene glycol used for the copolymer reaction. The implant surface was modified by etching with chloroform as previously described[12,22]. Surface topography of all modified rods was evaluated using scanning electron microscopy (SEM). Rods were sterilized by gamma irradiation at a minimum dose of 25 kGy (Synergy Health Ede, the Netherlands). The effect of gamma-radiation on the surface was evaluated using scanning electron microscopy (SEM).

Implantation of polymeric rods

Per rat, four rods were implanted in the subcutaneous space of the abdominal area. First pair of rods were inserted at 2 weeks after CKD induction and 5 weeks after BM transplantation, and left in place for 3 weeks. One week before rods extrusion another pair of rods were inserted for 1-week time point. Following a small horizontal incision of ca. 0.5 cm, a longitudinal subcutaneous pocket was formed where the rods were inserted. The incision was closed using 4-0 vicryl sutures (Johnson & Johnson, NJ, USA). The skin was closed intracutaneously. Rats directly received post operational analgesia via pre-operative injection of buprenorphine (0.01-0.05 mg/kg) and 2 oz gel cups with Carprofen (5 mg/kg) were placed into the cages for up to 3 days post-surgery. One or three weeks after insertion of the rods, tissue capsules were harvested and animals were euthanized by CO2 asphyxiation. In short, a longitudinal incision lateral to the rod was made and the tissue capsule was gently removed from the surrounding tissue. After harvesting, rods could easily be extruded from the tissue capsule.

Morphometric and histological analysis

Tissue capsules containing rods were fixed in 4% paraformaldehyde. After extrusion of the rods, tissue capsules were processed and embedded in paraffin. Serial cross sections of 5 mm of two parts of each tissue capsule were made for immunohistochemical and immunofluorescence analysis. To characterize the extracellular matrix, serial sections of each tissue capsule were stained with picrosirius red for collagen and Movat's stain for other extracellular matrix (ECM) components. Total collagen content was analyzed using QuickZyme Total Collagen Assay Kit (Biosciences, the Netherlands) according to the manufacturer protocol. In brief, five to ten 10 μm tissue sections were hydrolyzed by o/n incubation at 95°C in a heat block. Upon hydrolysis, 35 μl was used for collagen quantification. The assay measured the total amount of hydroxyproline present in the sample after 90 min of incubation time, which represents all collagen-types present in the sample. The assay results in a chromogen with an absorbance maximum at 570 nm.

Cellular composition of tissue capsules was characterized using immunohistochemistry, with antibodies against a-smooth muscle actin (1:1000; Dako M0851, CA, USA) for myofibroblasts, CD68 (1:300; Abcam Ab31630, Cambridge, UK) for macrophages and Ki67 (1:100; BD-Pharmigen 550609, CA, USA) for proliferating cells and visualized with 3.3¢-diaminobenzadine (DAB).

To visualize GFP^+ cells sections were stained with anti-GFP antibody (1:100; Abcam, ab13970, Cambridge, UK) with secondary Cy5 conjugated Goat anti-Chk IgY (1:500; Abcam ab97147, Cambridge, UK). For immunofluorescent staining of CD68 after primary antibody Alexa 568 conjugated goat anti mouse IgG1 (1:300; Molecular Probes A21124, OR, USA) was used. SMA was counterstained with Alexa 488 conjugated secondary mouse IgG2a (1:250; Molecular Probes A21131, OR, USA). Stem/progenitor cell-like population was stained with CD133 (primary ab 1:200; Abcam Ab19898, Cambridge, UK) and secondary goat anti rabbit IgG Alexa 488 (1:250; Molecular Probes A11008, OR, USA). Anti-inflammatory macrophages were visualized by the double staining of CD68 and CD163 (1:400; Immunologic 1105-C01, the Netherlands; secondary goat anti rabbit IgG Alexa 488 (1:250; Molecular Probes

A11008, OR, USA). Nuclei were visualized with ProLong™ Gold Antifade Mountant with DAPI (Thermo Fisher P369, MA, USA). Negative controls were obtained using an isotype antibody and in addition for all stainings a positive control was taken along.

All slides were digitized using an automated microscopic scanner (Pannoramic digital MIDI, 3DHISTECH, Budapest, Hungary). For the quantification of all immunofluorescence staining, the number of positive cells was counted in 8 random fields of view within the TC area at 60x ($CD68^+$ and $CD68^+/GFP^+$) or 120x (SMA^+/GFP^+; $SMA^+/GFP^+/CD68^+$; $CD68^+/CD163^+$ and $CD133^+/GFP^+/SMA^+$) magnification, from which the mean was calculated. Quantification of bright field Ki67 staining was performed with HistoQuant software (3DHISTECH) by calculating % DAB positive area from the total tissue capsule area.

Flow Cytometry and Blood and BM Analysis

The peripheral blood was withdrawn from rat tail vein into tubes containing 15% EDTA for FACS analysis. For the analysis of GFP^+ cells in the BM, complete BM was flushed out from femurs and tibia of rats post-lethality. Red blood cell lysis buffer (1.2 mL, Sigma, St Louis, MO, USA) was added into the tubes containing 0.1 mL blood and/or BM and incubated at 37^0C for 5 minutes followed by addition of 10 mL PBS and centrifugation to remove the lysed red blood cells. The cells (10^6 cells/mL) were resuspended in 50 mL FACS buffer (PBS containing 1% BSA and 0.01% sodium azide) and incubated with Hoechst antibodies (Thermo Fisher, MA, USA) for life/dead cell gating. GFP fluorescence on the surface was determined by fluorescence-activated cell sorting analysis (FACS, LSR II; BD Biosciences, CA, USA). Data were analyzed using FACS-Diva software (BD Biosciences, CA, USA).

RNA isolation, cDNA synthesis and qPCR

Total RNA was extracted from VSMCs using Trizol reagent (Invitrogen, CA, USA) according to the manufacturer's protocol. RNA was reverse transcribed by M-MLV First-Strand Synthesis system (Invitrogen, CA, USA), and used for quantitative analysis of rat genes (Supplementary Table 1) with an SYBR Green Master Mix (Applied Biosystems, CA, USA). Ribosomal protein S15 (RPS15) was used as standard housekeeping gene. The relative mRNA expression levels were determined using $2[-\Delta\Delta C(T)]$ method.

Statistical analysis

Results are expressed as mean±SEM and considered statistically significant for $P<0.05$. T tests and Mann-Whitney tests for parametric and nonparametric data, respectively, were used as appropriate.

Results

Surgical procedure

Generation of rats with GFP-labeled hematopoietic cells and chronic kidney disease

To investigate the contribution of BM derived cells to TC formation, we established a rat model where cells of the hematopoietic lineage expressed GFP. SD rats were transplanted with BM cells derived from transgenic GFP-SD rats. No immunological rejection occurred, as all of the experimental animals underwent BM-transplantation survived and demonstrated high engraftment of donor-derived GFP^+ cells. Percentage of GFP^+ cells was evaluated by FACS analysis of the peripheral blood at three time points: 1) 3 weeks after BM transplantation; 2) 6 weeks later, when the polymeric rods were implanted; and 3) when the polymeric rods were excised from the TC, another 3 weeks later. The percentages of GFP^+ BMCs in the peripheral blood of the rats at these 3 time points were 74±1.6%; 80±1.5%; and 77±3%, respectively. The percentage of GFP^+ cells in the BM at time of TC harvest was 72±3.6%.

Three weeks after BM transplantation, 17 rats underwent a 5/6 nephrectomy procedure from which 8 rats survived (47%). The healthy control group (WT) comprised of 10 animals with BM transplant but without the 5/6 nephrectomy procedure.

The CKD condition was established and persisted for the duration of TC formation. At the time of TC harvest, histological analysis of the remaining kidney of CKD rats revealed enlarged sclerotic glomeruli, dilated tubuli, regions of tubular necrosis and cast formation (Supplementary Figure 1). These structural changes coincided with elevated serum creatinine and BUN levels at the time of rod implantation and rod extrusion (mean creatinine levels: implantation—WT 0.4 mg/dL, vs. CKD 0.94 mg/dL, P=0.0001; extrusion—WT 0.48 mg/dL vs. CKD 1.1 mg/dL P=0.0001; mean BUN levels: implantation—WT 15.2 mg/dL vs. CKD 31.1 mg/dL, P=0.0007; extrusion—WT 18.6 mg/dL vs. CKD 40.25 mg/dL, P=0.0005).

The high mortality rate (53%) of CKD animals was primarily due to uremia as creatinine and blood urea nitrogen levels in these animals were very high, emphasizing the severity of 5/6 nephrectomy model (data not shown).

Implantation of the rods and TC harvest

Fabrication of implanted material was performed as previously described[12]. To create a homogeneous porous surface along the rod, for optimal inflammatory cell recruitment and organization of collagen and myofibroblasts, rods were etched with chloroform. Chloroform etching was verified using SEM (Supplementary Figure 2).

Two weeks after induction of CKD, 4 polymer rods were implanted into the subcutis of the rats in the abdominal area. TCs were harvested at 1- and 3-weeks after subcutaneous implantation of the rods. The study design is summarized in figure 1.

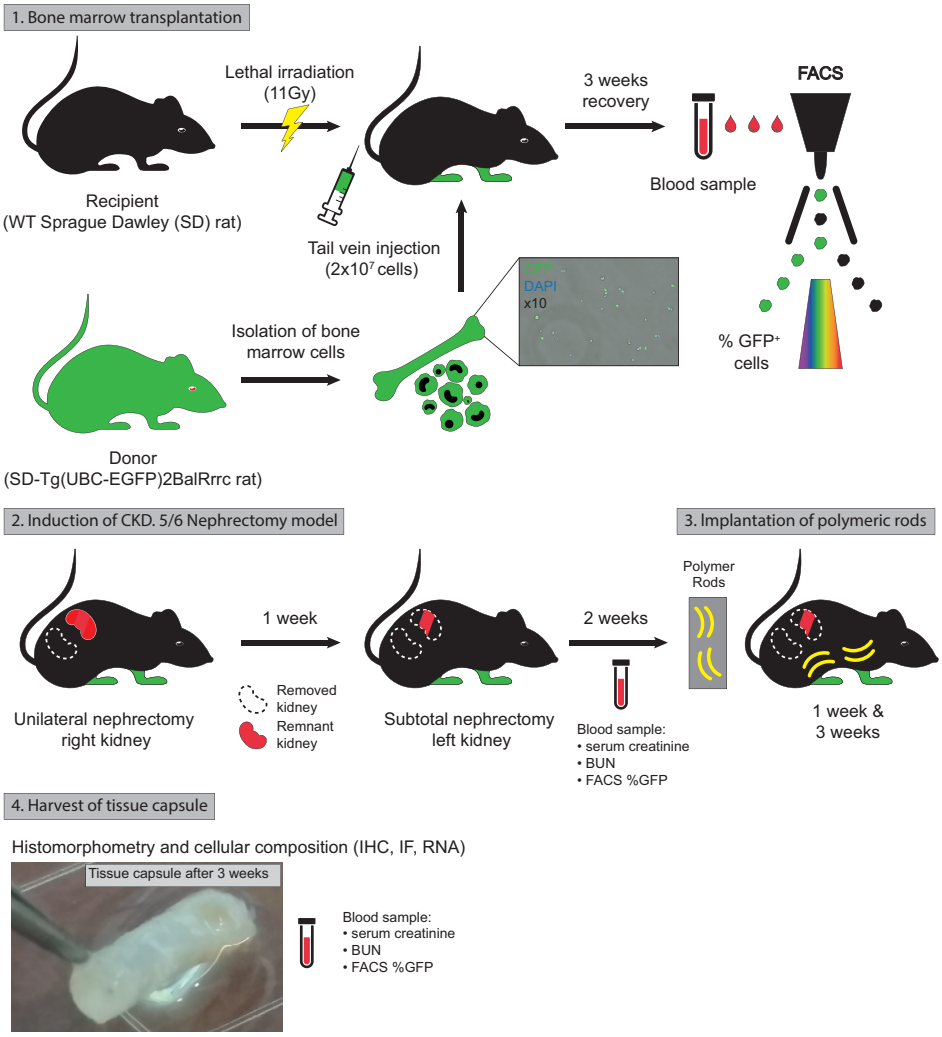

Figure 1. Schematic representation of the project work flow.
(1) 2*10^7 of total bone marrow cells harvested from transgenic Sprague Dawley (SD) rats ubiquitously expressing green fluorescent protein (GFP) were injected into the tail vein of wild-type (WT) SD recipient rats; n=27. Three weeks after the bone marrow reconstitution percentage of GFP$^+$ cells in the peripheral blood of recipient rats was measured by FACS analysis. (2) 2-step induction of chronic kidney disease (CKD); 1) unilateral right side nephrectomy and 2) 2/3 subtotal nephrectomy of the left kidney. Degree of CKD was confirmed by serum creatinine and blood urea nitrogen (BUN) levels 2 weeks after the procedure. (3) Polymeric rods were implanted into subcutaneous space of CKD and WT animals. (4) After 1 and 3 weeks implantation, rods together with formed fibrocellular tissue capsule were extruded and processed for further analysis. n=10 WT, n=8 CKD group.

Tissue capsule formation

Cellular organization within the TC gradually changed from a disorganized, highly nucleated structure at 1-week, to circumferentially aligned tissue at 3-weeks in both WT and CKD groups. TCs were mainly composed of extracellular matrix components (Figure 2a) and SMA$^+$ myofibroblasts (Figure 2b). The evolution of the TC formation was characterized by an initial accumulation of CD68$^+$ macrophages in proximity to the synthetic rod at the 1-week time point, whereas at 3-weeks CD68$^+$ cells were gradually dispersed through the entire TC volume (Figure 2c). Furthermore, the number of Ki67$^+$ proliferating cells at 3-weeks reduced by 40% and 67% (P=0.03) in WT and CKD animals, respectively, when compared to the 1-week time point (Figure 2d). The collagen density gradually increased as the TC maturated, forming a well-defined circular structure at 3-weeks in both WT and CKD animals (Figure 3a). Analysis of the total collagen content revealed increase in total collagen amount in the TCs at 3 weeks in both WT and CKD animals (WT: 54% increase, P=0.02; CKD: 61% increase, P=0.01) when compared to TCs obtained at 1 week after rod implantation (Figure 3b). No difference in collagen content was detected between WT and CKD animals, indicating that CKD state has no major influence on collagen synthesis in the TCs.

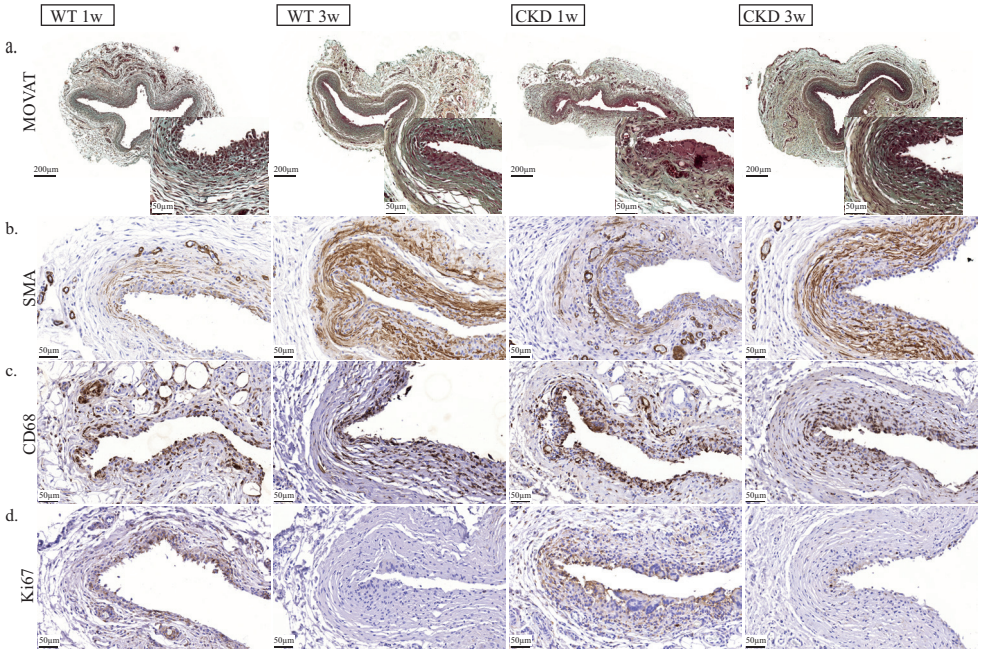

Figure 2. Cellular composition of tissue capsule at 1 and 3 weeks post-implantation. Immunohistochemical staining of (a) various constituents of connective tissues by MOVAT; (b) SMA$^+$ myofibroblasts, (c) CD68$^+$ macrophages and (d) Ki67$^+$ proliferating cells in the TC from healthy controls (WT) and chronic kidney disease (CKD) rats harvested at 1 and 3 weeks post-implantation. n=10 WT, n=8 CKD group.

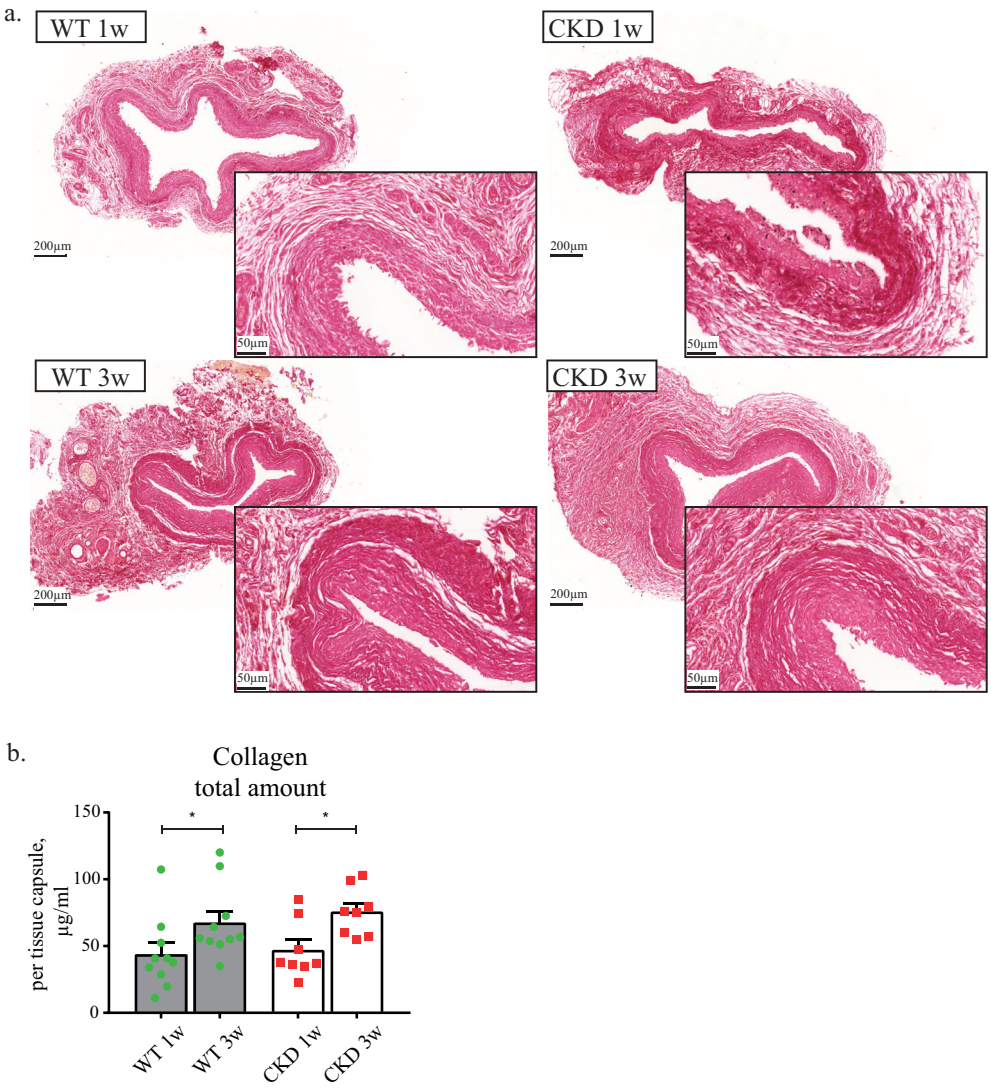

Figure 3. Changes in collagen content over the time course of tissue capsule maturation.
(a) Picrosirius red staining of the collagen. The collagen density gradually increased forming a well-defined circular structure at 3 weeks in both WT and CKD animals. (b) Analysis of the total collagen amount measured by QuickZyme Total Collagen Assay Kit. Significant increase in collagen content within WT and CKD groups was observed. (*) $P<0.05$; n=10 WT, n=8 CKD group.

A minority of inflammatory cells within TCs originates from the bone marrow

The number of CD68⁺ macrophages in the TCs at 3-weeks increased by 28% (P=0.03) and 82% (P=0.0006) in WT and CKD animals respectively, as compared to 1-week (Figure 4a,b).

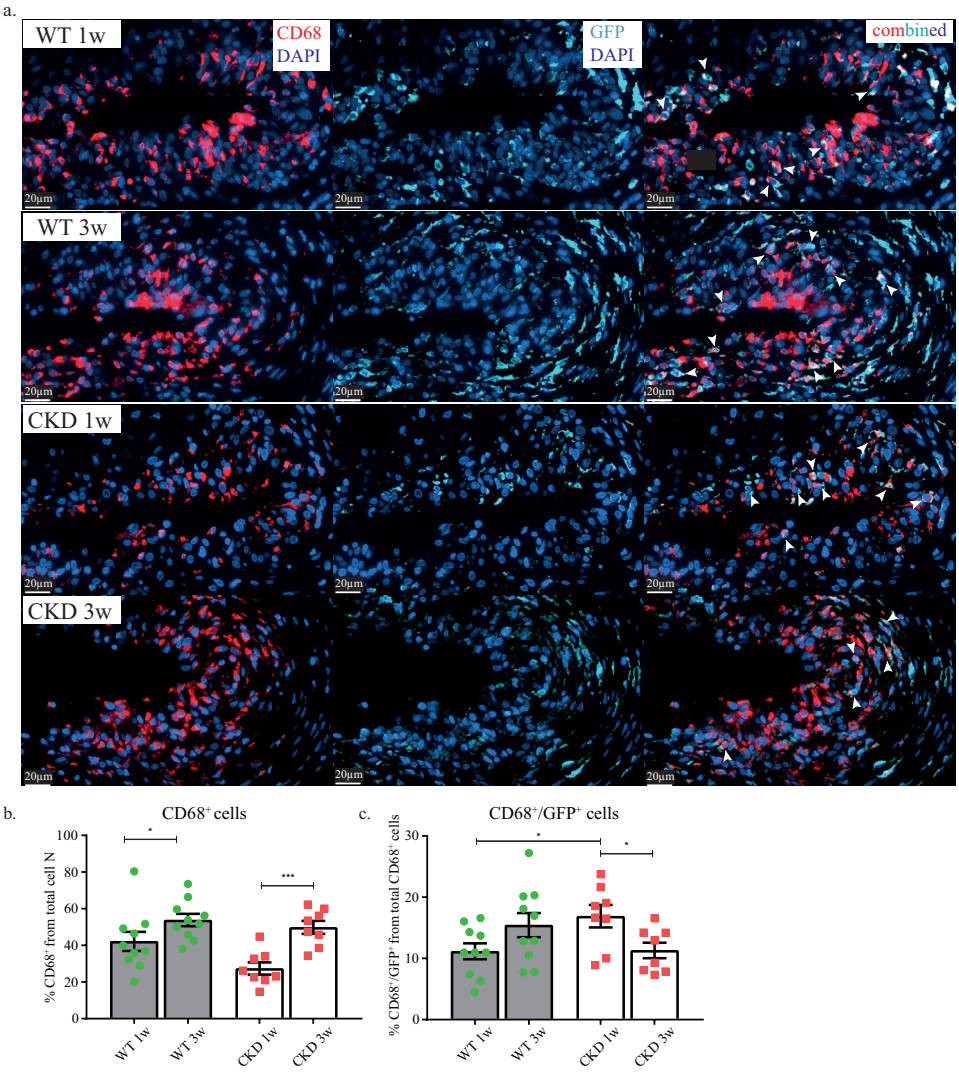

Figure 4. Macrophages in tissue capsule formation.

(a) Immunofluorescence staining of CD68⁺ macrophage marker (red color) and bone marrow derived GFP marker (light blue color). CD68⁺/GFP⁺ bone marrow derived macrophages (white arrows) was detected in the TC harvested at 1 and 3 weeks in WT and CKD group. (b) Quantification of total CD68⁺ macrophages within TC harvested at 1 and 3 weeks in WT and CKD animals. (c) Quantification of CD68⁺/GFP⁺ bone marrow derived macrophages from total CD68⁺ population. Nuclei DAPI (blue color). (*) P<0.05; (***) P<0.001; n=10 WT, n=8 CKD group.

Analysis of CD68⁺/GFP⁺ cells within TC at 1-week revealed that 11.2±1% and 16.9±2% of CD68⁺ cells originated from the bone marrow in WT and CKD group, respectively (Figure 4a,c). The percentage of BM-derived CD68⁺/GFP⁺ macrophages in TC at 3-weeks was 15.4±2% and 11.3±1.3% in WT and CKD group, respectively (Figure 4a,c). At 1-week time point, the percentage of CD68⁺ cells that expressed GFP was 1.5 times higher in the CKD group as compared to WT animals (P=0.03), whereas at 3-weeks this trend reversed (Figure 4c). The percentage of CD68⁺/GFP⁺ cells, from the CKD group, detected in the TC harvested at 3-weeks, was reduced by 33% as compared to the 1-week time point (P=0.02), (Figure 4c).

Contribution of bone marrow derived cells to myofibroblasts population in mature TCs

As described above, the TC harvested at 3-weeks was characterized by an increase in SMA⁺ myofibroblasts and accumulation of collagen and as compared to TCs obtained at 1-week after rod implantation (Figure 2b; 3a,b). Analysis of the TC harvested at 3-weeks revealed that 36% and 35% of SMA⁺ cells were originating from the BM as they were positive for GFP in WT and CKD group, respectively (Figure 5a,b). Moreover, 29% and 23% of SMA⁺/GFP⁺ myofibroblasts co-expressed a macrophage marker CD68 in the WT and CKD group, respectively (Figure 5a,c), suggesting a role for macrophage to myofibroblasts transition in TC formation.

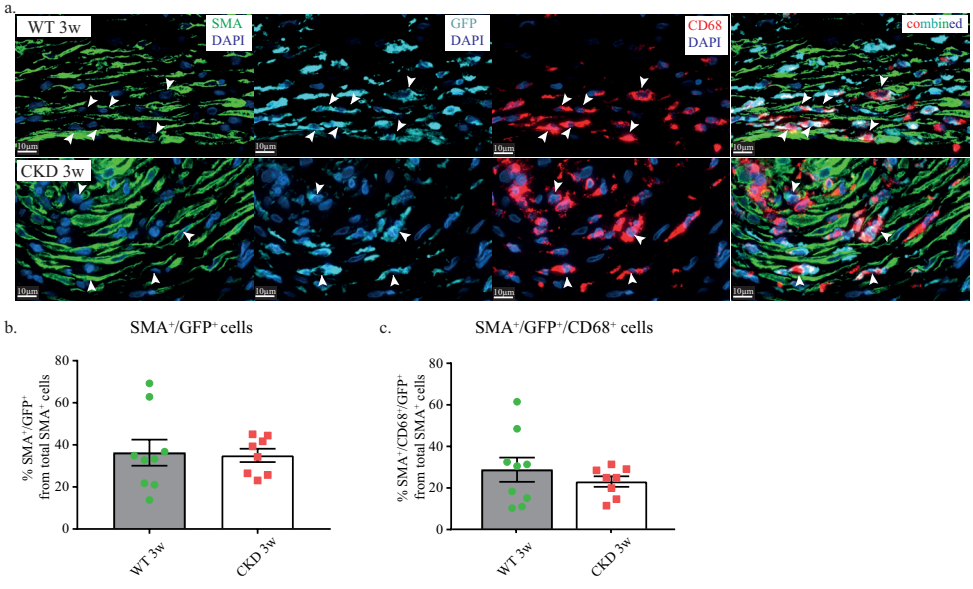

Figure 5. Macrophage to myofibroblasts transition.
(a) Immunofluorescence staining of SMA⁺ myofibroblasts (green color) co-expressing bone marrow derived GFP marker (light blue color) and CD68⁺ macrophage marker (red color). Population of SMA⁺/GFP⁺/CD68⁺ myofibroblasts (white arrows) was detected in TC at 3 weeks in both groups. Quantification of (b) SMA⁺/GFP⁺ and (c) SMA⁺/GFP⁺/CD68⁺ myofibroblasts from total SMA⁺ population within TC harvested at 3 weeks in WT and CKD group. Nuclei DAPI (blue color). n=9 WT, n=8 CKD group.

Tissue-resident macrophages in TC formation

There is accumulating evidence that tissue-resident macrophages orchestrate tissue-repair responses[23]. Immunohistochemical analysis of the TCs obtained at 3 weeks after rod implantation revealed that 53% and 58% of CD68$^+$ macrophages expressed the anti-inflammatory marker CD163$^+$, in WT and CKD animals respectively (Figure 6a,b). Gene expression analysis confirmed the repair-associated phenotype of these cells, as mRNA levels of transforming growth factor beta (TGFβ) in WT group was elevated by 2-fold (P=0.03), whereas mRNA levels of the anti-inflammatory cytokine IL10 in CKD group was 2-fold higher (P=0.04) in the TCs harvested at 3-weeks as compared to 1-week time point (Figure 6b).

Discrete population of cells positive for stem/progenitor-cell marker CD133

We observed a population of GFP$^+$/CD68$^-$ cells that accumulated predominantly at the outside border of the TC (Supplementary Figure 3). Interestingly, nearly all of these GFP$^+$/CD68$^-$ cells expressed CD133, a marker of progenitor cells of various origin[24], in both WT and CKD animals. Moreover, 24% of the CD133$^+$/GFP$^+$ cells co-expressed SMA (Figure 7a, b) indicating that BM derived hematopoietic stem cells can serve as direct precursors to myofibroblasts in mature TCs.

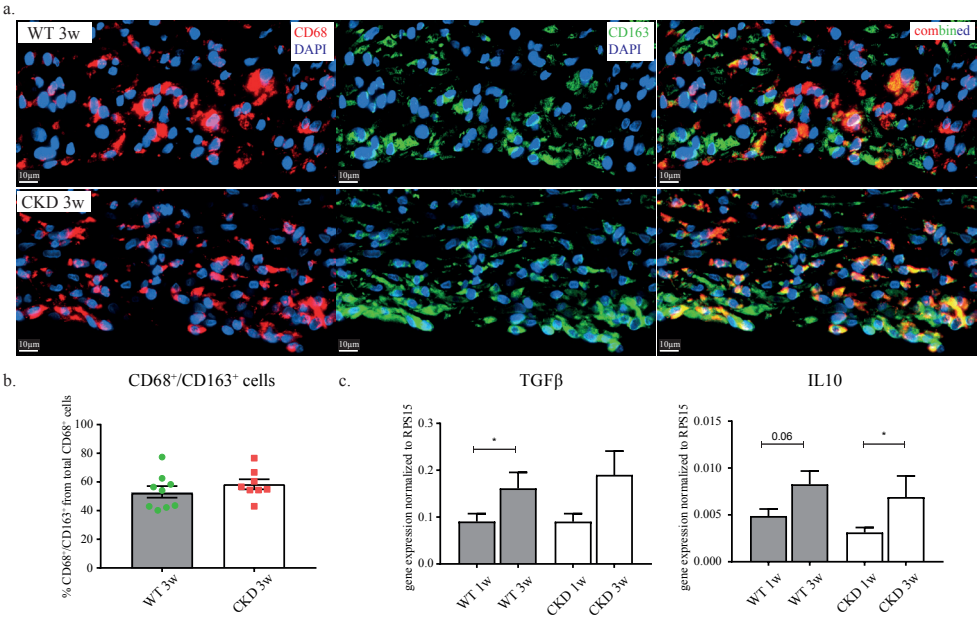

Figure 6. Tissue resident macrophages in tissue capsule formation.
(a) Immunofluorescence staining of CD68$^+$ macrophages (red color) positive for tissue resident marker CD163 (green color). (b) Quantification of the CD68$^+$/CD163$^+$ tissue resident macrophages from total CD68$^+$ cells. (c) Gene expression analysis of transforming growth factor beta (TGFβ) and anti-inflammatory cytokine IL10 in the TC at 1 and 3 weeks in WT and CKD group. Nuclei DAPI (blue color). (*) P=0.05; n=8 WT, n=8 CKD group.

Discussion

In the present study, we showed that both BM-derived and tissue-resident cells contribute to TC formation upon subcutaneous polymeric rod implantation. Surprisingly, only 13% of the macrophages within the TC originated from the BM, whereas 36% of the myofibroblast originated from BM precursors. A substantial number of SMA$^+$ bone marrow derived myofibroblasts co-expressed CD68, highlighting the role of the macrophage-to-myofibroblast transition in the formation of the TC. During the maturation of the TC, the cellular response predominantly displayed repair associated characteristics. Importantly, the CKD condition did not significantly affect the process of TC formation.

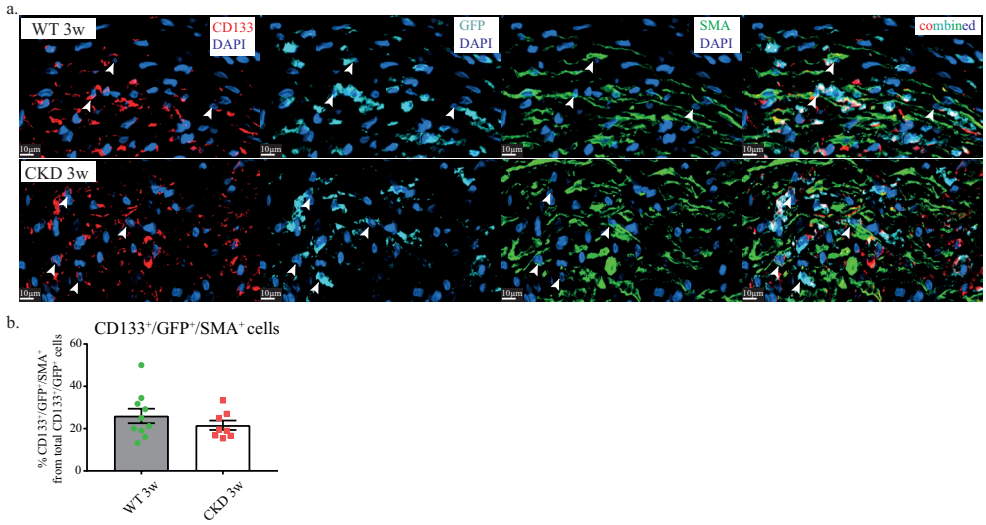

Figure 7. Expression of CD133 and GFP proteins by SMA$^+$ myofibroblasts in TC.
(a) Immunofluorescence staining of SMA$^+$ myofibroblasts (green color) originating from GFP$^+$ bone marrow (light blue color) derived CD133$^+$ stem/progenitor-cells (red color). CD133$^+$/GFP$^+$/SMA$^+$ cells (white arrows) were detected in the TC at 3 weeks in both experimental groups detected. (b) Quantification of CD133$^+$/GFP$^+$/SMA$^+$ within the TC at 3weeks in WT and CKD group. DAPI-nuclei blue. n=10 WT, n=8 CKD group.

Tissue-resident and BM-derived cells both contribute to the inflammatory response upon polymer rod implantation

Several studies have shown that the encapsulation of the foreign body is initiated with an inflammatory response, mainly through the activity of macrophages[14,15,25-27]. In this study, we also observed that along the inner border – adjacent to the polymeric rod – the tissue capsules were mainly composed of CD68$^+$ macrophages. Remarkably, only a minority of the macrophages within the TC originated from the bone marrow, as only 13% of the total CD68$^+$ population co-expressed GFP. Several studies suggest that cells within the local tissue environment, such as tissue-resident macrophages, also contribute to the foreign body response and play major role in the formation of

engineered tissue[28-30]. Tissue-resident macrophages consist of a mixture of embryonic- and adult-hematopoietic stem cell-derived macrophages, which have the capacity to self-renewal throughout adulthood[31,32].

Here, we show that the maturation of the TC is associated with a 40% increase in tissue-resident $CD68^+/CD163^+$ macrophages along with increase in IL10 and pro-fibrotic TGFβ mRNA levels within TCs. Besides, we did not observe a significant difference in $CD68^+/CD163^+$ macrophage population between CKD (46% of total macrophages) and WT animals (38%). Myofibroblast content was also similar between the groups. The latter most likely explains the similarity in collagen content in TCs as collagen is predominantly synthesized by (myo)fibroblasts.

Macrophages as precursors of myofibroblasts

During the development of the TC, we observed a gradual transition from granulation tissue towards circumferentially aligned SMA^+ myofibroblasts, whereas a substantial proportion of the myofibroblasts in the TCs were derived from hematopoietic BMCs. The ability of BM-derived cells to differentiate into smooth muscle-like cells was first described by Campbell and coworkers in their experimental work on TC formation in the peritoneal cavity[33]. Subsequent studies from the same group confirmed the plasticity of peritoneal macrophages and their ability to transdifferentiate from a myeloid to mesenchymal phenotype[34]. In our model, 26% of myofibroblasts originated from BM-derived macrophages, which illustrates the importance of macrophage-to-myofibroblast transition during the TC development.

Contribution of bone marrow progenitor cells to TC formation

Possibly, other than BM-derived and/or tissue resident macrophages can contribute to TC formation. A recent study by Wang *et al.* showed that $Sox10^+$ adult mouse stem cells found within the stroma of subcutaneous loose connective tissues, can contribute to encapsulation, fibrosis, and microvascularization of biomaterials upon implantation[35]. Interestingly, we observed a population of $CD133^+/GFP^+$ cells at the outer border of the TCs. Previous studies revealed that the membrane bound glycoprotein CD133 is expressed in mesenchymal stem cells (MSCs)[36] and stromal cells[37] within the BM. Both MSCs and stromal cells can give rise to human osteoblasts, adipocytes, chondrocytes as well as fibroblasts[38,39]. In this study, 24% $CD133^+/GFP^+$ cells were positive for SMA^+ suggesting that $CD133^+$ BM-derived cells can contribute to the myofibroblast population in mature tissue capsules.

CKD does not influence the cellular response during TC formation

As discussed above, the process of TC formation involves an acute inflammatory response, followed by chronic inflammation and fibrosis culminating in the encapsulation of the implanted biomaterial. CKD is a pro-fibrotic condition associated with tissue scarring as well as kidney and cardiac fibrosis[40-42]. Excessive TGFβ signaling, which has been implicated in epithelial cells and fibroblasts in CKD[41], can potentially enhance the process of TC formation in the subcutaneous space. On the other hand, CKD is associated with impaired function of both the innate and adaptive immune systems[17]. Circulating $CD34^+$ progenitor cells are markedly reduced in patients with CKD. In

addition, monocyte-macrophages are more prone to apoptosis in CKD patients[43], which could also negatively influence TC formation in CKD patients.

In the present study, we did not observe a significant effect of CKD on the cellular response upon implantation of the polymer rod. We hypothesize that the local foreign body response upon implantation of the polymer rod substantially differs from chronic inflammation and subsequent tissue fibrosis as observed in various organs of patients with CKD.

After only 3 weeks, tissue capsules were well matured, indicating the importance of the acute response and that the local environment within subcutaneous space is sufficient to maintain the process of TC formation.

Some aspects of our study require further discussion. One limitation in particular is the imperfect efficacy of the bone marrow transplantation, as only 75-80% of the cells in the peripheral blood were GFP^+ after BM-transplantation. As a consequence, the contribution of bone marrow derived cells in TC formation might be underestimated.

Our technology of tissue engineered blood vessels is aimed for patients with stage 5 of CKD which is defined as ESRD, when renal replacement therapy is required to survive. It needs to be emphasized that the 5/6-nephrectomy model used in the current study does not fully resemble ESRD, as the glomerular filtration rate (GFR) is this model is around 29-15% of normal (CKD stage 4). Thus, when extrapolating results to humans one should be cautious as TC formation in these rats might be slightly different when compared to dialysis patients. The pathophysiological mechanisms underlying CKD are also different between 5/6 nephrectomy animals and patients with CKD. Nevertheless, the 5/6-nephrectomy model in rats remains the most valuable and extensively investigated animal model mimicking human CKD[44-47].

Another limitation of this study is the inability to measure the mechanical strength of the TCs, an important parameter defining TC suitability for vascular grafting. However, a recent study performed in pigs demonstrates that the burst pressure and suture retention strength of the autologous TCs are sufficient to allow safe implantation in the arterial circulation[13].

Conclusion

This study illustrates that both BM-derived and resident cells contribute to the process of tissue response directed to a polymer rod that culminates in the formation of a collagen rich fibrocellular tissue capsule. BM-derived- as well as tissue resident macrophages serve as precursors of myofibroblasts in matured TCs. Notably, the presence of CKD does not significantly alter the process of TC formation, which supports the suitability of our autologous vascular tissue engineering approach for future clinical use in CKD patients.

Acknowledgements

This study was supported by a VIDI grant (016.156.328) awarded to J.I. Rotmans and funding from the National Institute of Health (EB012240 and HL083900) awarded to S. Li. We would like to thank Reshma A. Lalai for her excellent assistance in performing experiments and data analysis. Dr. Kei S. Iwamoto, from UCLA Radiation Oncology department for his excellent assistance in bone marrow transplantation experiments.

Flow cytometry was performed in the UCLA Jonsson Comprehensive Cancer Center (JCCC) and Center for AIDS Research Flow Cytometry Core Facility that is supported by National Institutes of Health awards P30 CA016042 and 5P30 AI028697, and by the JCCCJCCC, the UCLA AIDS Institute, the David Geffen School of Medicine at UCLA, the UCLA Chancellor's Office, and the UCLA Vice Chancellor's Office of Research.

Reference List

1. Diodato, M. & Chedrawy, E.G. Coronary artery bypass graft surgery: the past, present, and future of myocardial revascularisation. *Surgery research and practice* **2014**, 726158 (2014).
2. Kainz, A.*, et al.* Prediction of prevalence of chronic kidney disease in diabetic patients in countries of the European Union up to 2025. *Nephrology, dialysis, transplantation : official publication of the European Dialysis and Transplant Association - European Renal Association* **30 Suppl 4**, iv113-118 (2015).
3. Lloyd-Jones, D.*, et al.* Heart disease and stroke statistics--2010 update: a report from the American Heart Association. *Circulation* **121**, e46-e215 (2010).
4. Lee, T.*, et al.* Comparative analysis of cellular phenotypes within the neointima from vein segments collected prior to vascular access surgery and stenotic arteriovenous dialysis accesses. *Seminars in dialysis* **27**, 303-309 (2014).
5. Friedl, R.*, et al.* Intimal hyperplasia and expression of transforming growth factor-beta1 in saphenous veins and internal mammary arteries before coronary artery surgery. *The Annals of thoracic surgery* **78**, 1312-1318 (2004).
6. Rotmans, J.I.*, et al.* Hemodialysis access graft failure: time to revisit an unmet clinical need? *Journal of nephrology* **18**, 9-20 (2005).
7. Aslam, S., Vaida, F., Ritter, M. & Mehta, R.L. Systematic review and meta-analysis on management of hemodialysis catheter-related bacteremia. *Journal of the American Society of Nephrology : JASN* **25**, 2927-2941 (2014).
8. Roy-Chaudhury, P.*, et al.* Venous neointimal hyperplasia in polytetrafluoroethylene dialysis grafts. *Kidney international* **59**, 2325-2334 (2001).
9. Pashneh-Tala, S., MacNeil, S. & Claeyssens, F. The Tissue-Engineered Vascular Graft-Past, Present, and Future. *Tissue engineering. Part B, Reviews* (2015).
10. Yu, J.*, et al.* The effect of stromal cell-derived factor-1alpha/heparin coating of biodegradable vascular grafts on the recruitment of both endothelial and smooth muscle progenitor cells for accelerated regeneration. *Biomaterials* **33**, 8062-8074 (2012).
11. Geelhoed, W.J., Moroni, L. & Rotmans, J.I. Utilizing the Foreign Body Response to Grow Tissue Engineered Blood Vessels in Vivo. *Journal of cardiovascular translational research* **10**, 167-179 (2017).
12. Rothuizen, T.C.*, et al.* Tailoring the foreign body response for in situ vascular tissue engineering. *Tissue engineering. Part C, Methods* **21**, 436-446 (2015).
13. Rothuizen, T.C.*, et al.* Development and evaluation of in vivo tissue engineered blood vessels in a porcine model. *Biomaterials* **75**, 82-90 (2016).
14. Anderson, J.M., Rodriguez, A. & Chang, D.T. Foreign body reaction to biomaterials. *Seminars in immunology* **20**, 86-100 (2008).
15. Kenneth Ward, W. A review of the foreign-body response to subcutaneously-implanted devices: the role of macrophages and cytokines in biofouling and fibrosis. *Journal of diabetes science and technology* **2**, 768-777 (2008).
16. Westerweel, P.E.*, et al.* Impaired endothelial progenitor cell mobilization and dysfunctional bone marrow stroma in diabetes mellitus. *PloS one* **8**, e60357 (2013).
17. Kato, S.*, et al.* Aspects of immune dysfunction in end-stage renal disease. *Clinical journal of the American Society of Nephrology : CJASN* **3**, 1526-1533 (2008).
18. Teraa, M.*, et al.* Bone marrow alterations and lower endothelial progenitor cell numbers in critical limb ischemia patients. *PloS one* **8**, e55592 (2013).

19. Lois, C., Hong, E.J., Pease, S., Brown, E.J. & Baltimore, D. Germline transmission and tissue-specific expression of transgenes delivered by lentiviral vectors. *Science (New York, N.Y.)* **295**, 868-872 (2002).
20. van Koppen, A.*, et al.* Healthy bone marrow cells reduce progression of kidney failure better than CKD bone marrow cells in rats with established chronic kidney disease. *Cell transplantation* **21**, 2299-2312 (2012).
21. van Koppen, A., Verhaar, M.C., Bongartz, L.G. & Joles, J.A. 5/6th nephrectomy in combination with high salt diet and nitric oxide synthase inhibition to induce chronic kidney disease in the Lewis rat. *Journal of visualized experiments : JoVE*, e50398 (2013).
22. Damanik, F.F., Rothuizen, T.C., van Blitterswijk, C., Rotmans, J.I. & Moroni, L. Towards an in vitro model mimicking the foreign body response: tailoring the surface properties of biomaterials to modulate extracellular matrix. *Scientific reports* **4**, 6325 (2014).
23. Mantovani, A.*, et al.* The chemokine system in diverse forms of macrophage activation and polarization. *Trends in immunology* **25**, 677-686 (2004).
24. Yin, A.H.*, et al.* AC133, a novel marker for human hematopoietic stem and progenitor cells. *Blood* **90**, 5002-5012 (1997).
25. Miller, K.M., Huskey, R.A., Bigby, L.F. & Anderson, J.M. Characterization of biomedical polymer-adherent macrophages: interleukin 1 generation and scanning electron microscopy studies. *Biomaterials* **10**, 187-196 (1989).
26. Patino, M.G., Neiders, M.E., Andreana, S., Noble, B. & Cohen, R.E. Cellular inflammatory response to porcine collagen membranes. *Journal of periodontal research* **38**, 458-464 (2003).
27. Lucas, T.*, et al.* Differential roles of macrophages in diverse phases of skin repair. *Journal of immunology (Baltimore, Md. : 1950)* **184**, 3964-3977 (2010).
28. Davies, L.C., Jenkins, S.J., Allen, J.E. & Taylor, P.R. Tissue-resident macrophages. *Nature immunology* **14**, 986-995 (2013).
29. Okabe, Y. & Medzhitov, R. Tissue biology perspective on macrophages. *Nature immunology* **17**, 9-17 (2015).
30. Cailhier, J.F.*, et al.* Conditional macrophage ablation demonstrates that resident macrophages initiate acute peritoneal inflammation. *Journal of immunology (Baltimore, Md. : 1950)* **174**, 2336-2342 (2005).
31. Hashimoto, D.*, et al.* Tissue-resident macrophages self-maintain locally throughout adult life with minimal contribution from circulating monocytes. *Immunity* **38**, 792-804 (2013).
32. Dollinger, C.*, et al.* Incorporation of resident macrophages in engineered tissues: Multiple cell type response to microenvironment controlled macrophage-laden gelatine hydrogels. *Journal of tissue engineering and regenerative medicine* **12**, 330-340 (2018).
33. Campbell, J.H., Efendy, J.L., Han, C., Girjes, A.A. & Campbell, G.R. Haemopoietic origin of myofibroblasts formed in the peritoneal cavity in response to a foreign body. *Journal of vascular research* **37**, 364-371 (2000).
34. Mooney, J.E.*, et al.* Cellular plasticity of inflammatory myeloid cells in the peritoneal foreign body response. *The American journal of pathology* **176**, 369-380 (2010).
35. Wang, D.*, et al.* Sox10(+) adult stem cells contribute to biomaterial encapsulation and microvascularization. *Scientific reports* **7**, 40295 (2017).
36. Tondreau, T.*, et al.* Mesenchymal stem cells derived from CD133-positive cells in mobilized peripheral blood and cord blood: proliferation, Oct4 expression, and plasticity. *Stem cells (Dayton, Ohio)* **23**, 1105-1112 (2005).

37. Bakondi, B. & Spees, J.L. Human CD133-derived bone marrow stromal cells establish ectopic hematopoietic microenvironments in immunodeficient mice. *Biochemical and biophysical research communications* **400**, 212-218 (2010).
38. Bianco, P., Riminucci, M., Gronthos, S. & Robey, P.G. Bone marrow stromal stem cells: nature, biology, and potential applications. *Stem cells (Dayton, Ohio)* **19**, 180-192 (2001).
39. Jiang, Y.*, et al.* Pluripotency of mesenchymal stem cells derived from adult marrow. *Nature* **418**, 41-49 (2002).
40. Charytan, D.M.*, et al.* Increased concentration of circulating angiogenesis and nitric oxide inhibitors induces endothelial to mesenchymal transition and myocardial fibrosis in patients with chronic kidney disease. *International journal of cardiology* **176**, 99-109 (2014).
41. Xavier, S.*, et al.* Curtailing endothelial TGF-beta signaling is sufficient to reduce endothelial-mesenchymal transition and fibrosis in CKD. *Journal of the American Society of Nephrology : JASN* **26**, 817-829 (2015).
42. Mutsaers, H.A., Stribos, E.G., Glorieux, G., Vanholder, R. & Olinga, P. Chronic Kidney Disease and Fibrosis: The Role of Uremic Retention Solutes. *Frontiers in medicine* **2**, 60 (2015).
43. Bahlmann, F.H., Speer, T. & Fliser, D. Endothelial progenitor cells in chronic kidney disease. *Nephrology, dialysis, transplantation : official publication of the European Dialysis and Transplant Association - European Renal Association* **25**, 341-346 (2010).
44. Lu, H., Lei, X. & Klaassen, C. Gender differences in renal nuclear receptors and aryl hydrocarbon receptor in 5/6 nephrectomized rats. *Kidney international* **70**, 1920-1928 (2006).
45. Yang, H.C., Zuo, Y. & Fogo, A.B. Models of chronic kidney disease. *Drug discovery today. Disease models* **7**, 13-19 (2010).
46. Tsuprykov, O.*, et al.* The dipeptidyl peptidase inhibitor linagliptin and the angiotensin II receptor blocker telmisartan show renal benefit by different pathways in rats with 5/6 nephrectomy. *Kidney international* **89**, 1049-1061 (2016).
47. Bai, J.*, et al.* Netrin-1 attenuates the progression of renal dysfunction by blocking endothelial-to-mesenchymal transition in the 5/6 nephrectomy rat model. *BMC nephrology* **17**, 47 (2016).

Supplementary material

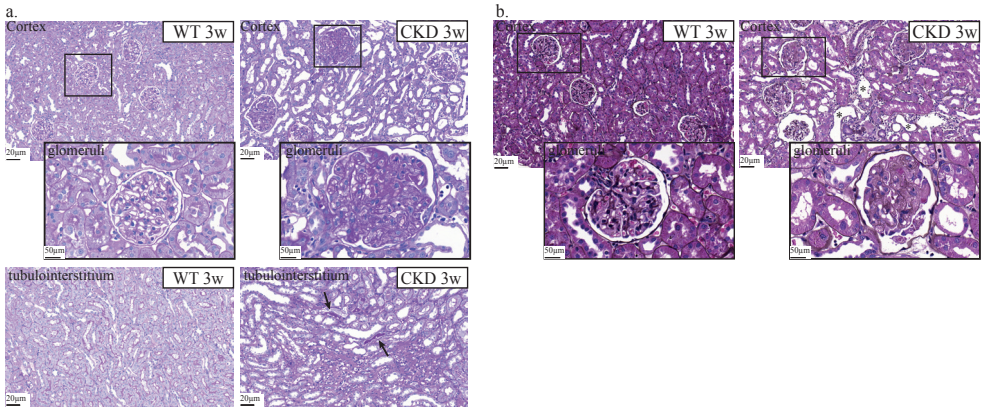

Supplementary Figure 1. Comparison of kidney histology between controls and rats underwent 5/6 nephrectomy.
(a.) Staining of kidney cortex with PAS (periodic acid-Schiff) highlights basement membranes of glomerular capillary loops. The capillary loops of WT glomerulus are well-defined an thin, as compared to enlarged sclerotic glomeruli, regions of tubular necrosis and tubular cast formation (black arrows) in CKD rats 5 weeks after 5/6 nephrectomy. (b.) Silver-stained kidney sections show pronounced glomerulosclerosis with dilated tubuli (black asterisks).

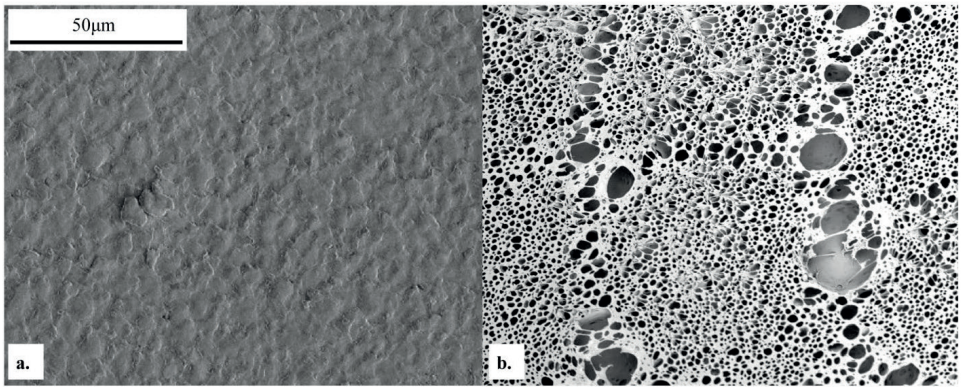

Supplementary Figure 2. Scanning electron microscopy images of (a) unmodified Pa300, (b) Pa300 chloroform-treated surface. Unmodified rods have smooth surfaces while chloroform etching resulted in porous structures on the surface.

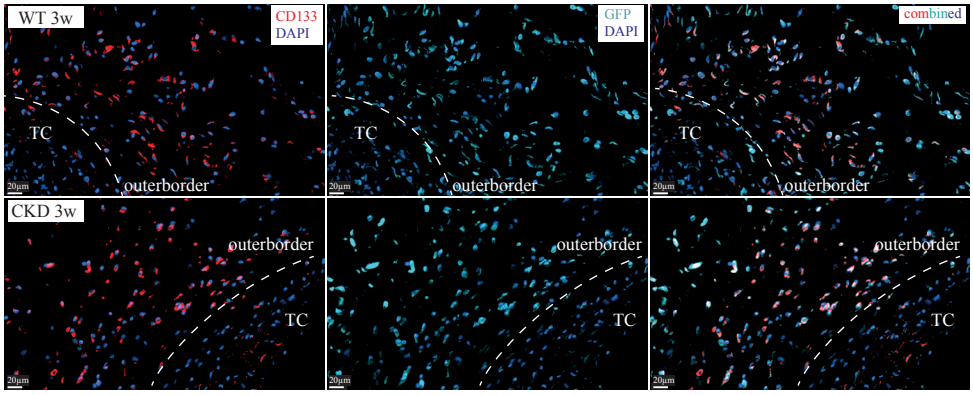

Supplementary Figure 3. Progenitor CD133⁺ bone marrow derived cells in tissue capsule.
Immunofluorescence staining of CD133⁺ stem/progenitor-cells (red color) originated from the GFP⁺ bone marrow (light blue color) detected in the TC at 3 weeks in WT and CKD groups. DAPI-nuclei blue.

Table 1 Primers used for *in vitro* experiments

Gene	Forward primer	Reversed primer
RPS15	CGTCACCCGTAATCCACC	CAGCTTCGCGTATGCCAC
IL10	AAAGCAAGGCAGTGGAGCAG	TCAAACTCATTCATGGCCTTGT
TGFβ	TGGCGTTACCTTGGTAACC	GGTGTTGAGCCCTTTCCAG